다양한 방사연단 조건을 갖는 고정 및 단순지지 부채꼴형 평판 진동에 대한 경계응력특이도의 영향

Influence of Boundary Stress Singularities on the Vibration of Clamped and Simply Supported Sectorial Plates With Various Radial Edge Conditions

김 주 우[1)]

Kim, Joo Woo

요 약 : 본 논문은 부채꼴형 평판의 원형연단이 고정되어 있거나 또는 단순지지 되어 있을 때 요각 모서리의 응력 특이도를 고려하여 자유 진동해를 최초로 구한 연구이다. Ritz방법을 이용하여 수직진동변위를 두가지 적합함수식으로 가정하였다. 본 연구에서는 부채꼴형 각도의 범위에 따른 엄밀한 진동수 및 수직진동 변위의 전형적인 등고선을 제시하였다.

ABSTRACT : This paper reports the first-of-its-kind free vibration solutions for sectorial plates having re-entrant corners causing stress singularities when the circular edge is either clamped or simply supported. The Ritz method is employed with two sets of admissible functions assumed for the transverse vibratory displacements. Accurate frequencies and normalized contours of the transverse vibratory displacement are presented for the spectra of sector angles.

핵 심 용 어 : Ritz 방법, 진동, 모서리 응력특이도, 부채꼴 평판, 고유진동수, 모드형상

KEYWORDS : Ritz method, vibration, corner stress singularities, sectorial plate, natural frequencies, mode shapes

1. Introduction

Documented in the literature spanning nearly two centuries are hundreds of technical publications explaining the free vibration characteristics of complete circular and annular plates with various support conditions along the circumferential boundaries. Extensive narratives of this large body of work have been chronicled in a summarizing monograph[(1)] and a series of review articles[(2,3,4)]. The scope of previous work done for the sectorial plate (see Fig. 1), in comparison, is quite narrow.

1) 정회원, 서울산업대학교 구조공학과 시간강사

본 논문에 대한 토의를 1999년 6월 30일까지 학회로 보내주시면 토의 회답을 게재하겠습니다.

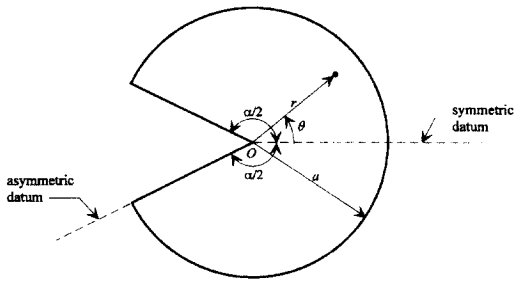

Fig.1 Geometric description of a sectorial Plate

Several authors have offered vibration data for thin sectorial and annular sector plates with various edge conditions on the circular and radial edges[5,6,7,8].

Exact solutions for frequencies and mode shapes have long been known to exist for sectorial plates having simply supported radial edges, with arbitrary conditions along the circular edge[1]. However, it has been shown[9,10] that such solutions are not applicable when the sector angle α exceeds 180^0 (forming a re-entrant corner, see Fig. 1). An exact solution for this situation involves non-integer order ordinary and modified Bessel functions of the first and second kinds, and particular relationships among the four constants of integration to satisfy the corner stress singularities properly. In spite of the existence of a number of semi-analytical solutions[11,12], one finds it intractable to derive exact solutions for sectorial plates with other combinations of clamped, simply supported, and free radial edges (*i.e.*, not both edges simply supported). In fact, little published vibration data exists for such sectorial plates with ($\alpha > 180^0$) or for the special case of a semi-circular plate ($\alpha = 180^0$), albeit a substantial amount of data exist for salient angles ($\alpha < 180^0$)[13]. In some recent papers incorporating corner stress singularity effects[9,10,14,15], accurate (five significant figure) frequencies and mode shapes were presented for sectorial plates with free circumferential edge and clamped or free radial edges, and for completely free circular plates with rigidly constrained or free V-notches.

The present work examines sectorial plates having either a clamped or simply supported circumferential edge, and arbitrary combinations of clamped, simply supported, and free radial edges, including stress singularity effects at the sharp vertex corner (see Fig. 1). For a very small notch angles, $360^0-\alpha$ (say, one degree or less), a deep, rigidly constrained, hinged, or free radial crack ensues. A Ritz procedure is employed in which the transverse displacement field is approximated as a hybrid set of trial functions consisting of a complete set of admissible algebraic-trigonometric polynomials in conjunction with an admissible set of corner functions that exactly model the singular vibratory moments which exist at the vertices of corner angles (α) which exceed 180 degrees[16,17]. The first set guarantees convergence to exact frequencies as sufficient terms are retained. The second set substantially accelerates the convergence of frequencies, which is demonstrated through convergence studies summarized herein. Accurate non-dimensional frequencies are presented as

the sector angle α is varied. To better understand the effects of the stress singularities existing in the title problem, normalized contour plots of the vibratory transverse displacements are studied for plates having sector angles a = 90^0, 180^0 (semi-circular), 270^0, 300^0, 330^0, 355^0, and 360^0 (radial line crack).

2. Methodology

Consider the polar coordinates (r, θ) originating at the vertex of the sectorial plate of radius, a, shown in Fig. 1. The transverse vibratory displacement w is defined in terms of these coordinates as follows:

$$w(r, \theta, t) = W(r, \theta)\sin \omega t \tag{1}$$

where t is time and w is the circular frequency of vibration. The boundary conditions for the various plates studied are identified according to the lettered edges shown in Fig. 2.

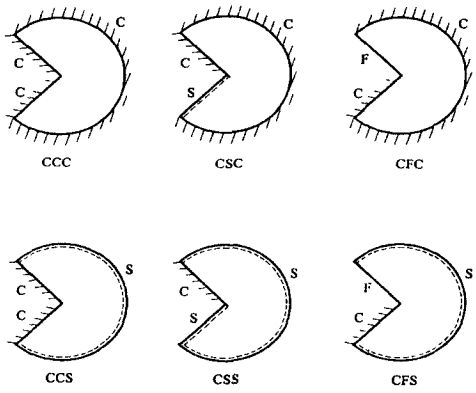

Fig. 2 Sectorial plates with various combinations of clamped, simply supported, and free edge conditions.

Displacement trial functions are assumed as the sum of two finite sets: $W = W_p + W_c$, where W_p are algebraic polynomials and W_c are corner functions. The admissible polynomials for the CCC, and CCS plates are written as

$$W_p = g_1(r, \theta)\Big(\sum_{m=0,2,4}^{M_1} \sum_{n=0,2,4}^{m} A_{mn} r^m \cos n\theta + \sum_{m=1,3,5}^{M_2} \sum_{n=1,3,5}^{m} A_{mn} r^m \cos n\theta \Big) \tag{2}$$

for the symmetric vibration modes, and

$$W_p = g_1(r, \theta)\Big(\sum_{m=2,4}^{M_1} \sum_{n=2,4}^{m} B_{mn} r^m \sin n\theta + \sum_{m=1,3,5}^{M_2} \sum_{n=1,3,5}^{m} B_{mn} r^m \sin n\theta \Big) \tag{3}$$

for the antisymmetric modes, and for the

CCC plate

$$g_1(r, \theta) = (r/a)^2[(\theta/\alpha)^2 - (1/2)^2]^2(a^2 - r^2)^2, \tag{4a}$$

CCS plate

$$g_1(r, \theta) = (r/a)^2[(\theta/\alpha)^2 - (1/2)^2]^2(a^2 - r^2), \tag{4b}$$

each of which is defined to satisfy the essential boundary conditions along the radial edges (see Fig. 1). Also indicated in Fig. 1 are datum lines utilized to define the symmetric and antisymmetric modes [Eqs. (2) and (3)]. No symmetry exists for the CSC, CSS, CFC, and CFS plates. Thus,

$$W_p = g_2(r,\theta)\Big(\sum_{m=0,2,4}^{M_1}\sum_{n=0,2,4}^{m} A_{mn} r^m \cos n\theta + \sum_{m=1,3,5}^{M_2}\sum_{n=1,3,5}^{m} A_{mn} r^m \cos n\theta + \sum_{m=2,4}^{M_3}\sum_{n=2,4}^{m} B_{mn} r^m \sin n\theta + \sum_{m=1,3,5}^{M_4}\sum_{n=1,3,5}^{m} B_{mn} r^m \sin n\theta\Big), \quad (5)$$

in which for the

CSC plate

$$g_2(r,\theta) = (r/a)^2(\theta/\alpha)(\theta/\alpha - 1)^2(a^2 - r^2)^2, \quad (6a)$$

CFC plate

$$g_2(r,\theta) = (r/a)^2(\theta/\alpha)(\theta/\alpha - 1)^2(a^2 - r^2), \quad (6b)$$

CFC plate

$$g_2(r,\theta) = (r/a)^2(\theta/\alpha)^2(a^2 - r^2)^2, \quad (6c)$$

CFS plate

$$g_2(r,\theta) = (r/a)^2(\theta/\alpha)^2(a^2 - r^2). \quad (6d)$$

In Eqs. (2), (3), and (5), A_{mn} and B_{mn} are arbitrary coefficients, and the values of m and n have been specially chosen to eliminate those terms which yield undesirable singularities at $r=0$, and yet, preserve the mathematical completeness of the resulting series as sufficient terms are retained. Thus, convergence to the exact frequencies is guaranteed when the series is employed in the present Ritz procedure.

The displacement polynomials [Eqs. (2), (3), and (5)] should, in principle, yield accurate frequencies. However, the number of terms required may be computationally prohibitive. This problem is alleviated by augmentation of the displacement polynomial trial set with admissible corner functions, which introduce the proper singular vibratory moments at the vertex corner formed by the radial edges (Fig. 1). The set of corner functions is taken as

$$W_c = G(r)\sum_{k=1}^{K} W^*_{c_k}, \quad (7)$$

where C_k are arbitrary coefficients, and $W^*_{c_k}$ are solutions of the fourth-order biharmonic, static equilibrium equation for bending of plates at acute corner angles(16)

$$W^*_{c_k}(r,\theta) = r^{\lambda_{k+1}}[a_k \sin(\lambda_k+1)\theta + b_k \cos(\lambda_k+1)\theta + c_k \sin(\lambda_k-1)\theta + d_k \cos(\lambda_k-1)\theta]. \quad (8)$$

The essential boundary conditions along the radial edges $\theta = \pm\alpha/2$ may be clamped [*i.e.*, $W(r, \pm\alpha/2) = \frac{1}{r}\frac{\partial W(r, \pm\alpha/2)}{\partial\theta} = 0$], simply supported [*i.e.*, $W(r, \pm\alpha/2) = M_r(r, \pm\alpha/2) = 0$], or free [*i.e.*, $V_r(r, \pm\alpha/2) = M_r(r, \pm\alpha/2) = 0$], where M_r and V_r are the usual radial moment and shear defined elsewhere(1). These conditions are used in Eq. (8) to construct a set of algebraic equations from which the values λ_k are obtained as roots of the vanishing determinants.

For the symmetric modes of the *CCC*

and CCS plates, $a_k=c_k=0$ in Eq. (8), and satisfaction of the clamped-clamped (C-C) radial edge conditions results in the following characteristic equation for the λ_k:

$$\sin \lambda_k\alpha=-\lambda_k\sin\alpha. \tag{9}$$

The corresponding corner function for the C-C edge conditions is

$$W^*_{c_k}(r,\theta) = r^{\lambda_{k+1}}\Big[-\frac{\cos(\lambda_k-1)\alpha/2}{\cos(\lambda_k+1)\alpha/2} \cos(\lambda_k+1)\theta+\cos(\lambda_k-1)\theta\Big]. \tag{10}$$

Similarly, for the antisymmetric modes of the CCC and CCS plates, $b_k=d_k=0$ in Eq. (10), and satisfaction of the C-C radial edge conditions results in the characteristic equation for the λ_k:

$$\sin \lambda_k\alpha=\lambda_k\sin\alpha. \tag{11}$$

The corner functions used for the antisymmetric modes are analogous to those defined for the symmetric ones in Eqs. (12), except the cosine functions are changed to sine functions, and vice-versa.

Imposition of the clamped-hinged (C-S) radial edge conditions yields the characteristic equation for the λ_k:

$$\sin 2\lambda_k\alpha=\lambda_k\sin 2\alpha, \tag{12}$$

and the corresponding C-S corner function

$$W^*_{c_k}(r,\theta) = r^{\lambda_k+1}\Big[\sin(\lambda_k+1)\theta - \frac{\sin(\lambda_k+1)\alpha/2}{\cos(\lambda_k+1)\alpha/2}\cos(\lambda_k+1)\theta - \frac{\sin(\lambda_k+1)\alpha/2}{\sin(\lambda_k-1)\alpha/2}\sin(\lambda_k-1)\theta + \frac{\sin(\lambda_k+1)\alpha/2}{\sin(\lambda_k-1)\alpha/2}\cos(\lambda_k-1)\theta\Big]. \tag{13}$$

Finally, the characteristic equation in λ_k for the clamped-free (C-F) radial edges is

$$\sin^2\lambda_k\alpha=\frac{4}{(1-\nu)(3+\nu)}-\frac{1-\nu}{3+\nu}\lambda_k^2\sin^2\alpha, \tag{14}$$

and the associated C-F corner function is

$$W^*_{c_k}(r,\theta) = r^{\lambda_{k+1}}[\sin(\lambda_k+1)\theta+\zeta_{1_k}\cos(\lambda_k+1)\theta + \zeta_{2_k}\sin(\lambda_k-1)\theta+\zeta_{3_k}\cos(\lambda_k-1)\theta] \tag{15}$$

with

$$\zeta_{1_k}=\frac{\mu_{1_k}}{\delta_k},\quad \zeta_{2_k}=\frac{\mu_{2_k}}{\delta_k},\quad \zeta_{3_k}=\frac{\mu_{3_k}}{\delta_k}, \tag{16a}$$

$$\mu_{1_k} = (\lambda_k-1)\eta_{2_k}\sin(\lambda_k+1)\frac{\alpha}{2} - (\lambda_k+1)\eta_{1_k}\cos(\lambda_k+1)\frac{\alpha}{2}\cos(\lambda_k-1)\alpha + (\lambda_k-1)\eta_{1_k}\sin(\lambda_k+1)\frac{\alpha}{2}\cos(\lambda_k-1)\alpha, \tag{16b}$$

$$\mu_{2_k} = (\lambda_k+1)\Big[\eta_{1_k}\cos(\lambda_k-1)\frac{\alpha}{2} - \eta_{2_k}\cos(\lambda_k-1)\frac{\alpha}{2}\cos(\lambda_k+1)\alpha - \eta_{3_k}\sin(\lambda_k-1)\frac{\alpha}{2}\sin(\lambda_k+1)\alpha\Big], \tag{16c}$$

$$\mu_{3_k} = (\lambda_k+1)\Big[\eta_{1_k}\sin(\lambda_k-1)\frac{\alpha}{2} + \eta_{2_k}\sin(\lambda_k-1)\frac{\alpha}{2}\cos(\lambda_k+1)\alpha - \eta_{3_k}\cos(\lambda_k-1)\frac{\alpha}{2}\sin(\lambda_k+1)\alpha\Big], \quad (16d)$$

$$\delta_k = (\lambda_k-1)\eta_{2_k}\cos(\lambda_k+1)\frac{\alpha}{2} - (\lambda_k+1)\eta_{1_k}\sin(\lambda_k+1)\frac{\alpha}{2}\sin(\lambda_k-1)\alpha - (\lambda_k-1)\eta_{1_k}\cos(\lambda_k+1)\frac{\alpha}{2}\cos(\lambda_k-1)\alpha, \quad (16e)$$

in which

$$\eta_{1_k} = \lambda_k(\nu-1)+(3+\nu),\ \eta_{2_k}=(\lambda_k+1)(\nu-1),\ \eta_{3_k} = (\lambda_k-1)(\nu-1). \quad (16f)$$

For the *CCC*, *CFC*, and *CSC* plates, the boundary function $G(r)=(a^2-r^2)^2$ in Eq. (7), whereas for the *CCS*, *CFS*, and *CSS* plates, $G(r)=(a^2-r^2)$. Some of the λ_k obtained from Eqs. (9), (11), (12), and (14) may be complex numbers, and thus, result in complex corner functions. In such cases, both the real and imaginary parts are used as independent functions in the present Ritz procedure outlined below.

In employing the Ritz method for free vibration problems, one has to construct the following frequency equations which, for the symmetric modes, are

$$\frac{\partial}{\partial A_{mn}}=(V_{\max}-T_{\max})=0, \quad \frac{\partial}{\partial C_k}=(V_{\max}-T_{\max})=0, \quad (17)$$

and similarly for the antisymmetric modes, using B_{mn} in place of A_{mn}. In Eqs. (17), the maximum strain energy, V_{max}, in the plate due to bending in a vibratory cycle is

$$V_{\max} = \frac{D}{2}\int_A[(\chi_r+\chi_\theta)^2 - 2(1-\nu)(\chi_r\chi_\theta-\chi_{r\theta}^2)]dA, \quad (18)$$

where $dA=rdrd\theta$, $D=Eh^3/12(1-\nu^2)$ is the flexural rigidity, h is the plate thickness, E is Young's modulus, ν is Poisson's ratio, and χ_r, χ_θ, and $\chi_{r\theta}$ are the maximum bending and twisting curvatures (and $\sin\omega t=1$ assumed in Eq. (1)):

$$\chi_r=\frac{\partial^2 W}{\partial r^2},\ \chi_\theta=\frac{1}{r}\frac{\partial W}{\partial r}+\frac{1}{r^2}\frac{\partial^2 W}{\partial\theta^2},\ \chi_{r\theta}=\frac{\partial}{\partial r}\left(\frac{1}{r}\frac{\partial W}{\partial\theta}\right). \quad (19)$$

The maximum kinetic energy is

$$T_{\max}=\frac{\rho\omega^2}{2}\int_A W^2 dA, \quad (20)$$

where ρ is the mass per unit area of the plate. The required area integrals in the dynamical energy Eqs. (18) and (20) are performed numerically, otherwise exact integrals are tractable when λ_k is real.

Substituting Eqs. (2)-(7), (10), (13), (15), and (16) into (17)-(20) yields a set of homogeneous algebraic equations involving the coefficients A_{mn} (or B_{mn})

and C_k. The roots of the vanishing determinant of these equations are a set of eigenvalues, which are expressed in terms of the nondimensional frequency parameter $\omega a^2\sqrt{\rho/D}$ commonly used in the plate vibration literature. Eigenvectors involving the coefficients A_{mn} (or B_{mn}) and C_k are determined in the usual manner by substituting the eigenvalues back into the homogeneous equations. Normalized contours of the associated mode shapes may be depicted on a $r-\theta$ grid in the sector plate domain, once the eigenvectors are substituted into Eqs. (2), (3), (5), and (7).

3. Convergence Studies

Having outlined the Ritz procedure employed in the present analysis, it is now appropriate to address the important question of convergence rate of frequencies, as various numbers of algebraic-trigonometric polynomials and corner functions are retained. In this section, convergence studies are summarized for sectorial plates with a 300 notch angle (*i.e.*, $\alpha = 330^0$). All of the frequency and mode shape data shown in the present and following sections are for materials having a Poisson's ratio (ν) equal to 0.3.

Consider the first six nondimensional frequencies $\omega a^2\sqrt{\rho/D}$ for the *CFC* (Table 1) sectorial plates ($\alpha = 330^0$). Numerical results are shown as 40, 60, 84, and 112 polynomial terms are retained in Eqs. (2), (3), or (5) in conjunction with 0, 1, 5, 10, 15, and 20 corner functions employed in Eq. (7). In these cases a larger number of polynomial terms is required due to the absence of symmetry of edge conditions.

Table 1. Convergence of frequency parameters $\omega a^2\sqrt{\rho/D}$ for a sectorial plate having clamped-free radial edges and clamped circum ferential edge ($\alpha = 330^0$)

Mode no.	No. of corner functions	Total number of terms in W_p			
		40	60	84	112
1	0	23.753	23.528	23.343	23.200
	1	23.475	23.321	23.170	23.046
	5	21.299	21.240	21.200	21.168
	10	20.989	20.980	20.977	20.975
	15	20.979	20.976	20.974	20.973
	20	20.978	20.975	20.974	20.973
2	0	28.773	27.884	27.190	26.700
	1	23.815	23.638	23.518	23.429
	5	22.659	22.602	22.565	22.540
	10	22.440	22.437	22.436	22.435
	15	22.438	22.436	22.435	22.435
	20	22.438	22.436	22.435	22.435
3	0	33.786	32.660	31.911	31.349
	1	33.401	32.226	31.458	30.897
	5	27.186	27.134	27.104	27.082
	10	26.992	26.988	26.985	26.983
	15	26.984	26.982	26.981	26.980
	20	26.984	26.981	26.980	26.980
4	0	41.849	40.181	39.094	38.298
	1	41.825	40.154	39.069	38.275
	5	34.672	34.581	34.513	34.465
	10	34.221	34.205	34.196	34.190
	15	34.192	34.186	34.183	34.181
	20	34.188	34.184	34.182	34.180
5	0	50.400	48.224	46.927	46.032
	1	50.277	48.066	46.790	45.918
	5	44.937	44.307	43.921	43.664
	10	42.477	42.438	42.415	42.402
	15	42.390	42.384	42.380	42.378
	20	42.382	42.380	42.378	42.377
6	0	59.704	57.256	55.836	54.882
	1	59.575	57.184	55.801	54.867
	5	57.282	55.286	54.192	53.513
	10	51.635	51.528	51.478	51.499
	15	51.454	51.428	51.415	51.407
	20	51.420	51.409	51.403	51.400

As indicated in Table 1, the lowest frequency mode of a *CFC* plate exhibits a slow upper bound monotonic decrease of $\omega a^2\sqrt{\rho/D}$ to an inaccurate value of 23.200, as the number of polynomial terms (W_p) is increased with no corner functions. That is, the polynomial series, albeit complete, is converging very slowly. An examination of the next five rows of data reveals that an accurate value to five significant figures is 20.973. With trial sets of 84 polynomials and 10 corner functions, three significant figure convergence of the lowest frequency mode is achieved. One can clearly see that by adding the first 20 corner functions to as few as 40 polynomials yields the value of 20.978, which is exact to four significant figures. Table 1 explains similar levels of convergence accuracy in the $\omega a^2\sqrt{\rho/D}$ values achieved by using hybrid trial set of admissible polynomials and corner functions apropos to sectorial plates with various boundary conditions. It should be noted that the *CFC* (Table 1) case is the one of the most challenging convergence studies (with regard to the number of corner functions required) among the six problems analyzed here, and that the other boundary condition cases required fewer corner functions to achieve the proper convergence of frequencies.

4. Frequencies And Mode Shapes

Tables 2 and 3 summarize the results of extensive convergence studies of the least upper bound frequency parameters $\omega a^2\sqrt{\rho/D}$ for the first six modes of sectorial plates with increasing sector angles $\alpha = 90^0$, 180^0, 270^0, 300^0, 330^0, 350^0, 355^0, and 360^0. Listed in Table 2 are frequency parameters for sectorial plates having clamped-clamped, clamped-simply supported, and clamped-free radial edge conditions along with a clamped circumferential edge (*i.e.*, *CCC*, *CSC*, and *CFC*), whereas shown in Table 3 are frequency data for plates with the same radial edge conditions and a simply supported circumferential edge (*i.e.*, *CCS*, *CSS*, and *CFS*). Frequency parameters corresponding to the antisymmetric modes are indicated by a superscript asterisk (*) as appropriate to the *CCS* and *CCC* plates. All frequency results are guaranteed upper bounds to exact values (typically accurate to the five significant figures shown in Tables 2 and 3). Hence, Tables 2 and 3 provide an accurate database of frequencies for sectorial plates having various edge conditions and notch angles against which future results using experimental or theoretical methods (such as finite element analysis) may be compared.

As can be expected, the frequency parameters of sectorial plates having a clamped circumferential edge are higher than those having a simply supported circumferential edge for all combinations of radial edge conditions. Generally speaking, one can conclude from Tables 2 and 3 that for the first six modes $\omega a^2\sqrt{\rho/D}$ decreases as the sector angle α increases.

Table 2. Frequency parameters $\omega a^2\sqrt{\rho/D}$ for sectorial plates having arbitrary radial edge conditions and clamped circumferential edge

Case	α (degrees)	Mode no. 1	2	3	4	5	6
CCC	90	48.786	87.774	104.88	136.93	164.57	180.71
	180	28.125	41.726*	58.677	71.950	78.375*	94.924*
	270	23.743	30.041*	39.399	50.241*	62.192	64.352
	300	23.246	28.005*	35.967	45.278*	55.590	63.347
	330	22.956	26.455*	33.277	41.389*	50.383	60.147*
	350	22.834	25.630*	31.790	39.238*	47.506	56.473*
	355	22.810	25.447*	31.450	38.745*	46.848	55.634*
	360	22.789	25.275*	31.133	38.287*	46.269	54.897*
CSC	90	41.726	78.375	94.922	125.20	151.87	167.87
	180	25.271	38.269	54.821	67.367	74.000	89.655
	270	22.575	27.884	37.143	47.787	59.588	62.368
	300	22.432	26.074	33.974	43.149	53.296	62.011
	330	22.376	24.718	31.481	39.506	48.368	57.995
	350	22.358	24.025	30.100	37.487	45.644	54.494
	355	22.355	23.875	29.783	37.025	45.020	53.691
	360	22.351	23.736	29.478	36.578	44.419	52.919
CFC	90	26.476	52.109	69.078	91.503	113.00	131.60
	180	21.501	29.295	43.458	59.486	61.193	74.420
	270	21.122	23.566	30.964	40.603	51.460	59.255
	300	21.083	22.811	28.724	37.010	46.375	56.688
	330	20.973	22.435	26.980	34.180	42.377	51.400
	350	20.880	22.326	26.028	32.610	40.161	48.466
	355	20.858	22.309	25.813	32.251	39.653	47.795
	360	20.837	22.296	25.606	31.903	39.163	47.147

*Antisymmetric modes

Table 3. Frequency parameters $\omega a^2\sqrt{\rho/D}$ for sectorial plates having arbitrary radial edge conditions and simply supported circumferential edge

Case	α (degrees)	Mode no. 1	2	3	4	5	6
CCS	90	37.457	72.951*	88.711	118.71	144.45*	159.53
	180	19.504	31.431*	46.601	58.548	64.544*	79.602*
	270	15.777	21.252*	29.442	39.092*	49.854	51.669
	300	15.348	19.503*	26.436	34.672*	43.916	50.743
	330	15.093	18.175*	24.092	31.229*	39.247	48.046*
	350	14.985	17.471*	22.802	29.333*	36.679	44.733*
	355	14.963	17.314*	22.508	28.900*	36.093	43.977*
	360	14.943	17.167*	22.232	28.496*	35.558	43.348*
CSS	90	31.431	64.545	79.607	107.97	132.65	147.55
	180	17.164	28.481	43.247	54.386	60.675	74.758
	270	14.830	19.454	27.527	36.973	47.591	49.861
	300	14.690	17.900	24.754	32.846	41.922	49.536
	330	14.631	16.737	22.585	29.624	37.506	46.167
	350	14.610	16.140	21.389	27.847	35.077	43.011
	355	14.606	16.010	21.115	27.441	34.522	42.288
	360	14.603	15.889	20.851	27.049	33.987	41.595
CFS	90	18.049	40.965	55.916	76.896	96.430	113.46
	180	13.828	20.707	33.180	47.359	49.023	60.807
	270	13.504	15.748	22.161	30.648	40.349	47.040
	300	13.478	15.085	20.214	27.470	35.789	45.061
	330	13.402	14.733	18.703	24.982	32.224	40.293
	350	13.335	14.620	17.881	23.606	30.257	37.657
	355	13.319	14.601	17.695	23.292	29.807	37.057
	360	13.303	14.585	17.516	22.988	29.373	36.476

*Antisymmetric modes

Shown in Figs. 3-5 are normalized displacement contours for the first three modes of sectorial plates with various conditions for $\alpha = 90^0$, 180^0, 270^0, 300^0, 330^0, 355^0, and 360^0. These contour plots are normalized with respect to the maximum transverse displacement component (*i.e.*, $-1 \le W/W_{max} \le 1$, where the negative values of W/W_{max} are depicted as dashed lines in Figs. 3-5, and the nondimensional frequencies shown correspond to the data listed in Tables 2 and 3). Contour lines are shown for W/W_{max}, ± 0.2, ± 0.4, ± 0.6, ± 0.8, ± 1. Nodal patterns of each mode are shown in Figs. 3-5 as darker contour lines of zero displacement ($W/W_{max} = 0$) during vibratory motion.

For *CCC* and *CCS* sectorial plates, a horizontal nodal line passes through the vertex of the notch in the antisymmetric mode 2. Thus, the singular vibratory stresses caused by the notch effect are considerably less, and fewer corner functions are required to achieve sufficiently accurate convergence of these modes. It is seen that a sharp notch ($a = 355^0$) causes almost radial nodal lines extending from the vertex of the notch to the circumferential edge in the symmetric mode 3 of the *CCC* and *CCS* sectorial plates. Interestingly, the radial nodal lines in the symmetric mode 3 shift slightly away from the vertex of a 90^0 notch ($a = 270^0$) in these cases.

The lowest frequency (*i.e.*, fundamental) symmetric mode of the *CCC* and *CCS* plates appear to be more strongly

influenced by the notch angle than the antisymmetric mode 2 and symmetric mode 3. In the fundamental mode, the sharp curvature and distortion of the nodal lines is quite apparent due to the notch effect, more so for the *CCS* plate than the *CCC* one. Given the absence of symmetry in the *CSC* and *CSS* displacement contours, their nodal patterns are rotated slightly in the clockwise direction in relation to the nodal patterns of the *CCC* and *CCS* plates, respectively.

It can also be seen that in the mode 3 of the *CFC* and *CFS* plates, the horizontal radial nodal line of the former plates appears slightly rotated from the horizontal in the clockwise direction in the latter plates. Across the board in Figs. 3-5, the W/W_{max} contours and nodal patterns of the sectorial plates are only slightly changed by the clamped or simply supported circumferential edge conditions. As expected, the contour lines $W/W_{max} = \pm 0.2$ occur closer to a simply supported circumferential edge than a clamped one, since in the latter both the normal displacement $[W(a, \theta)]$ and the bending slope $[\partial W(a, \theta)/\partial r]$ vanish.

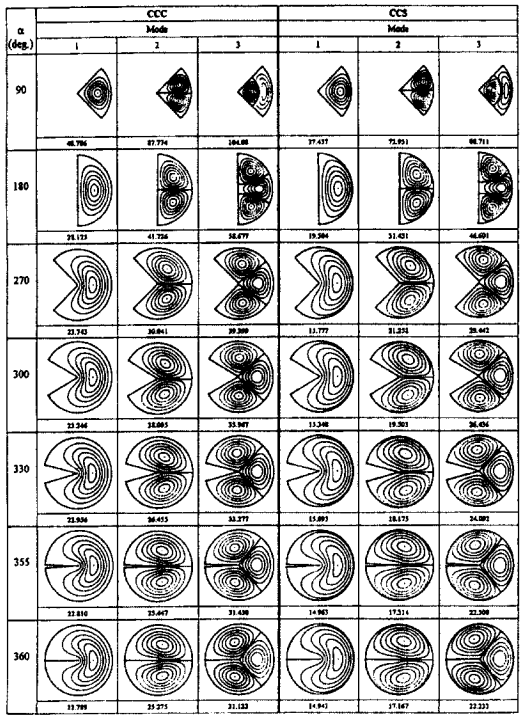

Fig. 3 Normalized transverse displacement contours (W/W_{max}) for the first three modes CCC and CCS sectorial plate

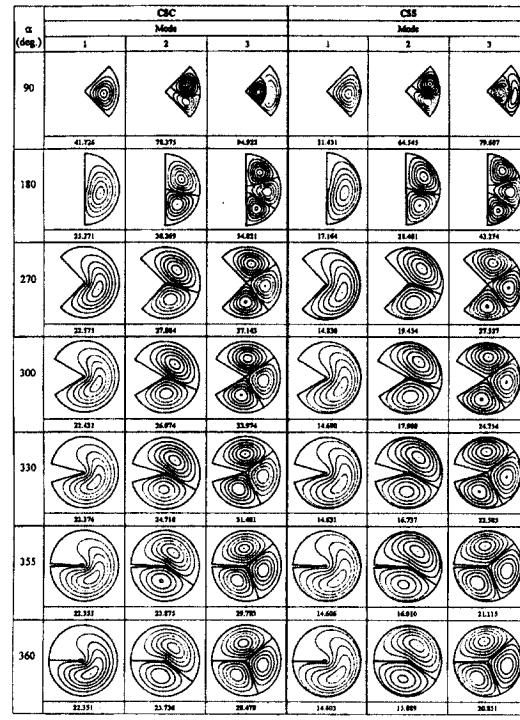

Fig. 4 Normalized transverse displacement contours (W/W_{max}) for the first three modes CSC and CSS sectorial plate

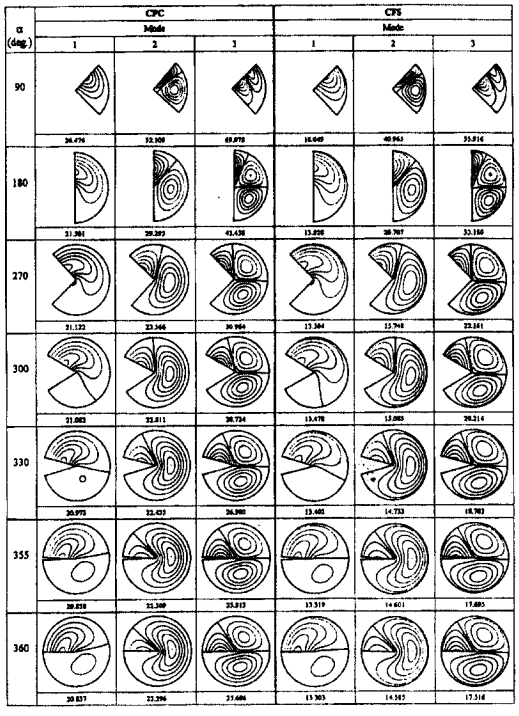

Fig. 5 Normalized transverse displacement contours (W/W_{max}) for the first three modes CFC and CFS sectorial plate

5. Concluding Remarks

Highly accurate frequencies and mode shapes for sectorial plates with a clamped or simply supported circumferential edge and arbitrary various radial edges have been obtained using a Ritz procedure in conjunction with classical thin-plate theory. In this approximate procedure, the assumed transverse displacement of the plate constitutes a hybrid set of complete algebraic-trigonometric polynomials along with corner functions that account for singular bending moments at the vertices of acute corner angles. The efficacy of such corner functions has been substantiated by an extensive convergence study of nondimensional frequencies of clamped and simply supported sectorial plates having various combinations of boundary conditions on the radial edges.

Detailed numerical tables have been presented, showing the variations of nondimensional frequencies (accurate to at least four significant figures) over a wide range of vertex angles α. On the whole, the numerical findings reveal that the constrained radial edges, including singularity effects, causes the first six $\omega a^2\sqrt{\rho}/D$ values to decrease as the sector angle α increases. This frequency decrease is observed to a larger extent in the higher modes than in the lower ones. Some exceptions to this overall trend have been discussed in the previous section.

Some new understanding has been offered here about the mode shapes of sectorial plates with clamped, simply supported, or free conferential and radial edges. As one examines the nodal patterns and normalized transverse displacement contours of the sectorial plates presented herein, it can be seen that a deep wide notch ($\alpha = 270^0$) or sharp crack ($\alpha = 355^0$) causes noticeably distorted and complicated nodal lines in the first three modes. Generally speaking, for $\alpha > 180^0$ highly localized bending moment stresses at the vertex of rigidly constrained, hinged, or free radial edges of sectorial plates may become detrimental in connection with vibration. This is because the singular stresses at the constrained vertex of sectorial plates with $\alpha \geq 355^0$ can become quite serious

during vibration by constituting an origin for crack propagation during fatigue.

The present variational Ritz approach is computationally effective for modeling the unbounded vibratory stresses, which exist at the sharp vertex corners of constrained radial edges of sectorial plates. Some fundamental mechanics understanding of the effect of these localized stresses on constrained sectorial plate dynamics can be obtained through careful examination of the frequency and mode shape data reported herein.

References

(1) Leissa, A. W., Vibration of Plates, NASA SP-160. Washington, D.C.: U.S. Government Printing Office, 1969 (Reprinted by The Acoustical Society of America, 1993).

(2) Leissa, A. W., Recent research in plate vibrations: classical theory, The Shock and Vibration Digest 9(10), 1977, pp. 13-24.

(3) Leissa, A. W., Plate vibration research, 1976-1980: classical theory, The Shock and Vibration Digest 13(9), 1981, pp. 11-22.

(4) Leissa, A. W., Recent studies in plate vibrations: 1981-1985, part I, classical theory, The Shock and Vibration Digest 19(2), 1987, pp. 11-18.

(5) Ben-Amoz, M., Note on deflections and flexural vibrations of clamped sectorial plates, ASME Journal of Applied Mechanics 26(1), 1959, pp. 136-137.

(6) Bhattacharya, A. P. and Bhowmic, K. N., Free vibration of a sectorial plate, Journal of Sound and Vibration 41(4), 1975, pp. 503-505.

(7) Maruyama, K. and Ichinomiya, O., Experimental investigation of free vibrations of clamped sector plates, Journal of Sound and Vibration 74(4), 1981, pp. 563-573.

(8) Mizusawa, T., Application of the spline element method to analyze vibration of annular sector plates, Journal of Sound and Vibration 149(3), 1991, pp. 461-470.

(9) Leissa, A. W., McGee, O. G., and Huang, C. S., Vibration of sectorial plates having corner stress singularities, ASME Journal of Applied Mechanics 60, 1993, pp. 134-140.

(10) Huang, C. S., Leissa, A. W., and McGee, O. G., Exact analytical solutions for the vibrations of sectorial plates with simply supported radial edges, ASME Journal of Applied Mechanics 60, 1993, pp. 478-483.

(11) Mizusawa, T., Vibration of thick annular sector plates using semi-analytical methods, Journal of Sound and Vibration 150(2), 1991, pp. 245-259.

(12) Harik, I. E. and Molaghasemi, H. R., Analytical solution to free vibration of sector plates, ASCE Journal of Engineering Mechanics 115(12), 1989, pp. 2709-2722.

(13) Kim, C. S., and Dickinson, S. M., On the free, transverse vibration of annular and circular, thin, sectorial plates subjected to certain complicating effects, Journal of Sound and Vibration 134, 1989, pp. 407-421.

(14) Leissa, A. W., McGee, O. G., and Huang, C. S., Vibrations of circular plates having V-notches or sharp radial cracks, Journal of Sound and Vibration 161(2), 1993, pp. 227-239.

(15) McGee, O. G., Leissa, A. W., Huang, C. S., and Kim, J. W., Vibrations of circular plates with clamped V-notches

or rigidly constrained radial cracks, Journal of Sound and Vibration 181(2), 1995, pp. 185-201.
(16) Williams, M. L., Surface stress singularities resulting from various boundary conditions in angular corners of plates under bending, Proceedings of the First U.S. National Congress of Applied Mechanics, 1951, pp. 325-329.
(17) Huang, C. S., Singularities in plate vibration problems, Ph.D. Dissertation, The Ohio State University, Columbus, Ohio, U.S.A., 1991.

(접수일자 : 1998년 9월 5일)